Functional analysis of light-harvesting-like protein 3 (LIL3) and its light-harvesting chlorophyll-binding motif in *Arabidopsis*

Kaori Takahashi[1], Atsushi Takabayashi[1,2], Ayumi Tanaka[1,2], Ryouichi Tanaka[1,2]

[1]Institute of Low Temperature Science, Hokkaido University, 060-0819, Sapporo, Japan

[2]Japan Core Research for Evolutionary Science and Technology, Sapporo 060-0819, Japan

*Running title: *Functional analysis of light-harvesting-like protein 3*

To whom correspondence may be addressed: Ryouichi Tanaka, Institute of Low Temperature Science, Hokkaido University, N19W8, Kita-ku, Sapporo, 060-0819, JAPAN, Tel: +81-11-706-5494; E-mail: rtanaka@lowtem.hokudai.ac.jp

Keywords: chloroplast; light-harvesting-like protein; isoprenyl metabolism

Background: The light-harvesting-complex (LHC) motif is an amino acid consensus sequence found in various thylakoid proteins.

Results: Modification and replacement of the transmembrane domain encompassing the LHC motif of a plant protein retains its membrane-anchoring function but impairs its protein-protein interaction.

Conclusion: This domain functions for membrane anchoring and complex formation.

Significance: This study provides new insights regarding the function of the LHC motif.

ABSTRACT

The light-harvesting complex (LHC) constitutes the major light-harvesting antenna of photosynthetic eukaryotes. They contain a characteristic sequence motif which is termed an LHC motif consisting of 25-30 mostly hydrophobic amino acids. This motif is shared by a number of transmembrane proteins from oxygenic photoautotrophs which are termed LILs. To gain insights into the functions of LIL proteins and their LHC motifs, we functionally characterized a plant LIL protein, LIL3. This protein was previously shown to stabilize geranylgeranyl reductase (GGR), a key enzyme in phytol biosynthesis. It is hypothesized that LIL3 functions to anchor GGR to membranes. First, we conjugated the transmembrane (TM) domain of LIL3 or that of ascorbate peroxidase to GGR and expressed these chimeric proteins in an *Arabidopsis* mutant lacking LIL3 protein. As a result, the transgenic plants restored phytol-synthesizing activity. These results indicate that GGR is active as long as it is anchored to membranes even in the absence of LIL3. Subsequently, we addressed the question why the LHC motif is conserved in the LIL3 sequences. We modified the TM domain of LIL3, which contains the LHC motif, by substituting its conserved amino acids (E171, N174 and D189) with alanine. As a result, the *Arabidopsis* transgenic plants partly recovered the phytol biosynthesizing activity, however, in these transgenic plants, the LIL3-GGR complexes were partially dissociated. Collectively, these results indicate that the LHC motif of LIL3 is involved in the complex formation of LIL3 and GGR, which might contribute to the GGR reaction.

Protein domains represent functional units of protein sequences. Domains are often conserved during evolution. In some instances,

specific regions of genomic DNA encoding domains have been duplicated, modified and transferred within or between genomes. Genomic modifications such as these have contributed towards the evolution of proteins. From an analysis perspective, domains can be recognized through characterization of sequence footprints or "motifs". Currently, numerous protein motifs have been identified by the analysis of protein sequences that are deposited in public sequence databases (1, 2). In addition to providing invaluable information regarding protein functions, these motifs also provide clues pertaining to protein evolution. The light-harvesting-complex (LHC) motif, or which is alternatively called the chlorophyll *a/b* motif, is a widely distributing motif among the genomes of oxygenic photosynthetic organisms (3-7) and was first identified in plants (8). The LHC motif plays essential roles in LHC, providing ligands for the binding of chlorophyll and carotenoids, and also serves as a structural backbone for LHC (9).

The LHC motif is not only identified in the protein sequences for LHC, but it is also found in many other proteins from oxygenic photosynthetic organisms (1, 2, 6, 7). These proteins are collectively called light-harvesting-like (LIL) proteins (3-7). Unlike LHC, LIL does not appear to be involved in light harvesting, although some of the LIL proteins appear to be at least temporarily associated with the photosynthetic apparatus (8, 10-13).

Both photosynthetic eukaryotes and cyanobacteria contain multiple LIL proteins. For example, the model cyanobacterium, *Synechocystis* sp. PCC6803 contains five different types of LIL proteins (9, 14), while *Arabidopsis* contains at least eight different types (5). The LHC motif sequences are well conserved among all types of LIL proteins. On the contrary, sequences residing outside of the LHC motifs are not conserved among different types of LIL proteins, indicating that different types of LIL proteins bear different functions (6, 7). Among various LIL proteins, ferrochelatase (FC) and LIL3 have clearly assigned functions. FC is responsible for the final step of heme biosynthesis, in which this enzyme inserts Fe^{2+} into protoporphyrin IX (15). LIL3 is involved in the stabilization of geranylgeranyl reductase (GGR), which is the enzyme that is responsible for phytol formation (16). A few other types of LIL proteins have been characterized and their functions have been proposed. Cyanobacterial LIL proteins are hypothesized to be involved in chlorophyll turnover (17, 18) or stabilization of photosystem 1 (19). The ELIP protein, which is alternatively called LIL1, is reported to be functionally associated with seed germination (20). Both ELIP (13) and SEP (21) are suggested to be involved in the response of plants to light stresses. Even though LIL proteins have been extensively studied, we still have limited understanding regarding the functions of their LHC motifs. At least three specific functions have been postulated for the LHC motif: membrane anchoring, providing binding sites of tetrapyrroles, and facilitating protein-protein interactions (5, 22). The function of the LHC motif of cyanobacterial FC has been studied at both the *in vivo* and *in vitro* levels (22-24). Although removal of the LHC motif from the FC sequence did not effect its catalytic activity, it resulted in a dissociation of the dimeric FC into monomers (22) and in the increased turnover of FC reaction (24). These results indicate that the LHC motif does not participate in the FC reaction. Instead, the LHC motif contributes to the formation of dimers and it is possibly involved in the regulation of FC reactions by controlling monomer-dimer transitions (24). To the best of our knowledge, the function of the LHC motif still remains to be elucidated for other LIL proteins. As a result, it is not clear whether the LHC motifs of LIL proteins have common functions or not.

In order to gain a better understanding regarding the functions of the LHC motif, we functionally characterized the LHC motif with *Arabidopsis* LIL3 protein in this study. LIL3 is a chloroplastic protein which contains two putative transmembrane (TM) helices, one of which encompasses an LHC motif (5). LIL3 is shown to interact with geranylgeranyl reductase (GGR), which catalyzes the reduction of geranylgeranyl-diphosphate (GGPP) to form phytyl-diphosphate (PDP), which is a key reaction leading to α-tocopherol, chlorophyll (phytylated chlorophyll: Chl-phy), and phylloquinone (Fig. 1). In addition, this

enzyme catalyzes the reduction of the geranylgeranyl side chain of chlorophyll to phytol (25, 26). The *Arabidopsis* genome encodes two LIL3 isoforms, which are designated as LIL3:1 and LIL3:2. Both isoforms are similar in sequence and exhibit 76% identity at the amino acid level. The LIL3 isoforms consist of the N-terminal region (120-130 amino acids) which is predicted to be soluble, and two transmembrane (TM) helices (ca. 90 amino acids) at their C terminus, the first of which contains a well-conserved LHC motif. In the *Arabidopsis lil3:1/lil3:2* double mutant lacking both LIL3 isoforms, GGR levels are significantly reduced (16). Accordingly, this mutant accumulates unusual chlorophyll species containing incompletely saturated side chains (see Fig. 1 for formulas): including geranylgeranylated chlorophyll (Chl-GG), dihydrogeranylgeranylated chlorophyll (Chl-DHGG) and tetrahydrogeranylgeranylated chlorophyll (Chl-THGG). In contrast, wild-type (WT) plants almost exclusively synthesize phytylated chlorophyll (Chl-phy)(16). Since a knock-out mutation of a single gene encoding either LIL3:1 or LIL3:2 only leads to a slight reduction in the GGR levels (16), it is most likely that LIL3:1 and LIL3:2 are functionally redundant. A yeast two-hybrid assay and blue-native polyacrylamide gel electrophoresis (BN-PAGE) analysis demonstrate that LIL3 and GGR interact with each other (16). Taken together, it was shown that LIL3 stabilizes GGR by a direct interaction.

In order to analyze the function of an LHC motif, it would be desirable to use an experimental system in which a functional impairment of an LHC motif is readily detectable. However, it has not always been possible to observe dysfunction of LIL proteins in LIL-deficient mutants (21). For other LIL proteins, a complex and sophisticated experimental system is required to observe the effects of LIL protein dysfunction (20, 27-29). On the contrary, a defect in the function of LIL3 is easily detectable by observing GGR levels and the Chl-phy levels (16). Thus, it is expected that *Arabidopsis lil3* mutants are capable of serving as an ideal system to enable the functional characterization of an LHC motif. Here, we describe the functional analysis of the LIL3 protein and its LHC motif using the *Arabidopsis lil3* mutant as a model system. It should be noted that for this study, we utilized a transgenic approach in plants rather than adopting the yeast split ubiquitin system that was used in our previous study (16). This approach was chosen because the plant system is expected to provide more-physiologically-relevant functional information regarding the function-structure relationship of LIL3 and its LHC motif. Such information pertaining to the functionality of LIL3 is difficult to obtain with the yeast system.

In this study, we introduced a modification in the LIL3 sequence and assessed its effects by overexpressing the modified *LIL3* gene in the *lil3:1/lil3:2* double mutant. Furthermore, we constructed a chimeric protein by conjugating GGR with the membrane-spanning domain of LIL3 (we designated this domain as TM_{LIL3}). For comparison, we also fused the membrane-spanning domain of thylakoid-bound ascorbate peroxidase (we designated this region as TM_{APX}), which we consider a non-LIL protein representative, to GGR. If the LIL3 protein functions to anchor GGR to membranes, a fusion of a membrane-spanning domain to GGR should functionally complement the lack of LIL3. The results suggest that anchoring GGR to membranes fulfills the function of LIL3. Furthermore, we found that an alteration of the LHC motif results in partial dissociation of GGR-LIL3 complexes and a substantial reduction of GGR activity. Taken together, we propose that the TM domain of LIL3 possesses a dual function to anchor GGR to membranes and to also oligomerize this enzyme.

EXPERIMENTAL PROCEDURES

Plants -The *Arabidopsis lil3:1/lil3:2* mutant was isolated from a Ds transposon-tagged mutant pool of the Nossen ecotype (16). Plants were grown at 23 °C under continuous light conditions [~80 μmol m^{-2} s^{-1}] as previously described (16). Counting from the top, the fourth whorl of the leaves was harvested 4 weeks after germination for the extraction of pigments, RNA, and protein.

Chlorophyll measurement - Chlorophyll was extracted from frozen leaves with cold acetone

and subjected to HPLC analysis as described previously (16).

Construction of Arabidopsis transgenic plants - For the construction of *Arabidopsis* transgenic plants overexpressing FLAG-tagged LIL3:2, cDNA for the full-length LIL3:2 was PCR amplified with a specific primer set that was designed to incorporate a FLAG-tag (DYKDDDDK) coding sequence into the PCR product. Likewise, for the construction of *Arabidopsis* transgenic plants expressing the amino-acid substituted LIL3:2 sequence in which three conserved amino acid residues were substituted with alanine (E171A, N174A and D189A), GAA to GCA, AAT to GCT and GAT to GCT substitutions were incorporated by an overlapping PCR method. The modified LIL3:2 cDNA fragments were cloned into pGreenII-0229 vector (30) together with the cauliflower mosaic virus 35S promoter, the omega sequence and the nopaline synthase terminator. For the construction of GGR-TM_{LIL3} or GGR-TM_{APX} expressing plants, sequences encompassing the full-length GGR sequence (1 to 1401 of the At1g74470 sequence), its own 5'UTR (-83 to −1) and 3'UTR (from 1402 to 1562) were separately amplified by PCR. The amplified fragments were subsequently fused with another DNA fragment coding for the transmembrane domain of LIL3:2 (corresponding to the nucleotides 499 to 774, which was counted from the initiation codon) or that for the transmembrane domain of ascorbate peroxidase (corresponding to the nucleotides 1105 to 1278) by an overlapping PCR method. The amplified PCR fragments were then cloned into the pENTR4-dual vector (Invitrogen) and the sequences were subsequently transferred to the pEarleyGate100 vector (31) by the Gateway recombination system (Invitrogen). The T-DNA region of the aforementioned binary plasmids were introduced into the *lil3:1/lil3:2* double mutant (16) by Agrobacterium-mediated transformation, with the exception for the LIL3:2-FLAG-expressing plasmid. This plasmid was introduced into the *lil3:2* mutant (16) of *Arabidopsis*.

Immunoblotting - For immunoblotting, total leaf proteins were extracted from the fourth whorl of 4-week-old plants with extraction buffer containing 50 mM Tris-HCl pH 8.0, 1.5% DTT, 12% Sucrose, and 2% LDS. Ten microliters of extracts, corresponding to 1 mg of leaf material, were separated on a 14% polyacrylamide gel and subsequently electroblotted to PVDF membrane. LIL3 protein and GGR protein was detected with an anti-GGR antiserum using the ECL-Plus immunodetection kit according to the manufacturer's instructions (GE Healthcare).

Immunoprecipitation - A single selected transgenic line expressing LIL3:2-FLAG was used for chloroplast isolation. Thylakoid membranes were isolated according to the method of Salvi et al (32). Standard procedures for the purification of the LIL3 complex containing LIL3:2-FLAG were followed. Specifically, isolated chloroplasts from approximately 120 plants were solubilized in buffer containing 1% α-dodecyl maltoside (α-DM), 10mM MOPS and 4mM MgCl2. Solubilized proteins were then incubated with FLAG-cross-linked NHS beads (Tamagawa Seiki Co. Ltd.) using a rotator for 2h at 4°C. The beads were washed with the same buffer, and then incubated with the DYKDDDDK-peptide containing buffer (Wako Chemicals) for 30 min.

BN-PAGE Analysis - For BN-PAGE analysis, thylakoid membranes were isolated from the leaves (containing 3-8 μg of chlorophyll) of four-week-old plants. Leaves were homogenized by mortar and pestle in the leaf grinding medium containing 0.45M sorbitol, 20 mM Tricine/KOH pH8.4, 10 mM EDTA, 10 mM $NaHCO_3$ and 0.1% (wt/vol) BSA. The homogenate was initially centrifuged at 1,000 x g at 4°C for 1 min. The supernatant was then recovered and centrifuged again at 3,000 x g at 4°C for 5 min. The pellet was washed twice with the washing medium containing 0.3M sorbitol, 20 mM Tricine/KOH pH7.6, 5 mM $MgCl_2$ and 2.5 mM EDTA. The green pellet was suspended in the solubilization buffer containing 50 mM imidazole-HCl (pH 7.0), 20% glycerol, 5 mM 6-aminocaproic acid and 1 mM EDTA, and was mixed with an equal volume of 2% (wt/vol) α-DM solution. Solubilized membrane proteins were then separated by 5–14% acrylamide gradient gels according to the method of Wittig et al. (33). SDS-PAGE was performed as described previously (34).

Alignment of amino acid sequences - Amino acid sequences of representative LIL3 proteins

and those of *Arabidopsis* Lhcb1.1 were aligned by the MUSCLE software developed by Edgar (35) with its default parameters. The accession numbers of the amino acid sequences are as follows: LIL3:1 (*Arabidopsis*, NP_567532), LIL3:2 (*Arabidopsis*, NP_199522), Brassica1 (*Brassica oleracea*; ABD64919.1), Brassica2 (*Brassica oleracea*: ABD65018.1), Oryza1 (*Oryza sativa* BAG92255.1, Oryza2 (*Oryza sativa* BAD08011.1), Chlamydomonas (*Chlamydomonas reinhardtii* XP_001699421.1), Physcomitrella1 (*Physcomitrella patens*: XP_001756081.1), Physcomitrella2 (*Physcomitrella patens*: XP_001782647.1), Lhcb1.1 (*Arabidopsis thaliana*: NP_564340.1).

RESULTS

Isolation of GGR-LIL3 complexes - In our previous study, we showed that LIL3 interacts with GGR forming a few protein complexes, whose sizes are estimated to range between 160 to 250 kD (16). In order to obtain a further insight into the function of LIL3, we analyzed the protein compositions of the LIL3-GGR complexes. We expressed a FLAG-tagged LIL3:2 protein in the *Arabidopsis lil3:2* mutant and purified protein complexes using anti-FLAG antibody-conjugated magnetic beads. Isolated LIL3-GGR complexes were analyzed by blue-native polyacrylamide gel electrophoresis (BN-PAGE) and SDS-PAGE (Fig. 2). The isolated LIL3:2-containing complex was subsequently resolved by SDS-PAGE, which yielded two major bands (Fig. 2A). Mass spectroscopic analyses determined that these bands represent LIL3:1 and LIL3:2; both of which are estimated to be 30 kD, and GGR (47 kD). The results indicated that the major constituents of the isolated fraction are heteromeric complexes consisting of LIL3:1, LIL3:2 and GGR. The isolated complexes were separated into several major bands in the BN-PAGE analysis (Fig. 2B). In order to assign each band, we analyzed the isolated complexes with two-dimensional BN-PAGE/SDS-PAGE analysis (Fig. 2C). The protein profile was in good accordance with those obtained by immunoblotting analysis of the whole cell extracts, which were probed with anti-GGR and anti-LIL3 antibodies (16). Collectively, these data indicate that the isolated complexes reflect the protein compositions of the pre-purified LIL3-GGR complexes.

In the BN-PAGE analysis, we ran two molecular weight markers, NativeMark Unstained Protein Standard (Invitrogen: LC0725) and HMW Native Marker Kit (GE Healthcare: 17-0445-01), alongside the isolated protein complexes on the BN-PAGE gel (Fig. 2B). Due to the nature of native gel electrophoresis, the migration of protein complexes is largely influenced by the surface charges and the structure of protein complexes. As a result, the migration patterns of protein complexes in a native PAGE gel does not always correlate with the molecular weight of these complexes. In our analysis, the two representative molecular weight markers showed significant differences in their migration patterns. The major protein complex was estimated to be approximately 230 kD according to the NativeMark Unstained Protein Standard. On the other hand, the same complex was estimated to be 190 kD according to the HMW Native Marker Kit.

In order to gain further information regarding the composition of the LIL3-GGR complexes, the isolated LIL3-GGR complexes were analyzed by the combination of BN-PAGE and SDS-PAGE (Fig. 2C). Both of the largest LIL3-GGR and the major (second-largest) LIL3-GGR complexes appear to be solely composed of LIL3 and GGR proteins. On the contrary, the third largest band seems to consist of LIL3, while the fourth largest band seems to only consist of GGR. It is likely that the protein which we assigned as GGR oligomers and monomers were dissociated from the LIL3-GGR complexes during electrophoresis, because the protein was purified using the anti-FLAG antibody-conjugated beads which interact with the FLAG tag conjugated with LIL3. On the other hand, it is not clear whether the protein entities which we assigned LIL3 oligomers and LIL3 monomers are present *in vivo*. It should be noted that non-specific signals were detected above GGR signals in our two-dimensional analysis. It is likely that these signals were the result of human keratin contamination. Taken together, these results indicate that the major LIL3-GGR complexes are composed of the oligomers of LIL3 and GGR.

Subsequently, we analyzed the intra-organelle localization of LIL3 and GGR. Isolated chloroplasts were further separated by sucrose density gradient centrifugation into three different fractions enriched for thylakoid membranes, envelope membranes and stromal components, respectively. Immunoblotting analyses revealed that LIL3 was exclusively detected in the thylakoid membrane fraction (Fig. 3). Likewise, the majority of GGR was detected in the same fraction (Fig. 3). A trace amount of GGR was also detected in the envelope fraction. It is possible that our envelope fraction contained a small amount of thylakoid membranes, which might have resulted in the trace detection of GGR and LHCB1 (thylakoid marker) in this fraction. Considering that the envelope membrane only constitutes a minor fraction of total chloroplast membranes, which is estimated at only 2% of total membrane fraction (36), it is concluded that a vast majority of GGR is localized in thylakoid membranes.

Membrane-anchored GGR is stabilized in the absence of LIL3 - Although LIL3 has been shown to be necessary for the stabilization of GGR (16), the exact functional role of LIL3 was still not known. Considering that GGR lacks predictable hydrophobic domains (25) although it is mainly localized on thylakoid membranes (see Fig. 3), we hypothesized that LIL3 anchors GGR to membranes, and that this anchoring stabilizes GGR. If this hypothesis were correct, a direct fusion of a transmembrane (TM) domain to GGR would substitute the function of LIL3. In order to assess this hypothesis, we fused the putative TM domain of LIL3 (hereafter referred to as TM_{LIL3}), to GGR and constitutively expressed this chimeric protein (hereafter referred to as GGR-TM_{LIL3}) in the *Arabidopsis lil3:1/lil3:2* double mutant lacking LIL3:1 and LIL3:2 (see Fig. 4 for the overview of the experimental scheme). The GGR-TM_{LIL3} expressing lines exhibited enhanced growth and greener leaves in comparison to the *lil3:1/lil3:2* double mutant (Fig. 5). These data clearly indicated that GGR-TM_{LIL3} was capable of complementing the phenotype of the mutant.

To further assess the phytol-synthesizing activity in the GGR-TM_{LIL3} expressing lines, we analyzed the compositions of Chl species that are conjugated with incompletely reduced side chains (Chl-GG, Chl-DHGG and Chl-THGG) and those with the completely reduced side chain (Chl-phy). (We found that the compositions of the side chains for Chl *a* were well correlated with those for Chl *b* in all plants used in this study. Therefore, we only show the results of Chl *a* for simplicity.) WT plants almost exclusively synthesize Chl-phy, while the Chl-phy level is less than 5% of the total Chl level in the *lil3:1/lil3:2* double mutant (Fig. 6C). Instead, the major Chl species in this mutant is Chl-GG, which constitutes nearly 80% of the total Chl (Fig. 6C). The Chl-phy levels in the GGR-TM_{LIL3} overexpressing lines have been recovered to approximately 20% of the total Chl *a* level (Fig. 6C). Concomitantly, the levels of Chl-GG were substantially reduced to 30% of total Chl in the GGR-TM_{LIL3} overexpressing lines. These results indicate that the phytol-synthesizing activity is partially restored in the GGR-TM_{LIL3} overexpressing lines. Immunoblotting analysis showed that the GGR-TM_{LIL3} lines accumulate a substantial level of this chimeric protein, which is approximately half of the wild-type GGR levels (Fig. 6A). These results showed that conjugating the TM_{LIL3} domain increases the stability of GGR.

To test whether the TM_{LIL3} domain stabilizes GGR by anchoring, or through another specific function, we fused the membrane-spanning domain of ascorbate peroxidase (APX), which we referred to as TM_{APX}, to the C terminus of GGR and overexpressed them under the control of CaMV 35S promoter in the *lil3:1/lil3:2* double mutant (see Fig. 4). It has been previously shown that TM_{APX} is not involved in the catalytic mechanism of APX, and just functions to tether the catalytic domain of APX to thylakoid membranes (37). If TM_{APX} stabilizes GGR in a similar manner as TM_{LIL3}, it would indicate that anchoring GGR to membranes stabilizes GGR. We found that the growth of the GGR-TM_{APX} expressing lines was recovered and their leaves become greener when compared to the *lil3:1/lil3:2*double mutant (Fig. 5). In addition, the proportion of Chl-phy was higher (ca. 40%) in these lines than that of the *lil3:1/lil3:2* double mutant (ca. 5%) (Fig. 6C). In three independent GGR-TM_{APX} expressing lines, GGR-TM_{APX} levels were significantly

increased when compared to GGR levels in the *lil3* double mutant (Fig. 6B). These results show that TM_{APX} also stabilizes GGR, indicating that anchoring GGR to membranes increases the stability of GGR. Taken together, these results demonstrate that the function of LIL3 includes the anchoring of GGR to membranes.

The stabilizing effect of TM_{APX} appears to be greater in the GGR-TM_{APX} lines than that of TM_{LIL3} in the GGR-TM_{LIL3} expressing lines (Fig. 6A and 6B). One possible explanation is that TM_{APX} has less interference with the structure of GGR, because TM_{APX} contains a single membrane-spanning domain, while TM_{LIL3} contains two. As a result, it is possible that TM_{APX} might have a more compact structure.

It should be noted that the GGR-TM_{LIL3} and GGR-TM_{APX} expressing plants also accumulate a low level of endogenous GGR protein which is equivalent to that of the double mutant (Fig. 6A and 6B). These results indicate that overexpression of modified GGR-TM_{LIL3} or GGR-TM_{APX} does not affect the stability of endogenous GGR. Thus, we conclude that the chimeric proteins (GGR-TM_{LIL3} or GGR-TM_{APX}) contribute to the recovery of Chl-phy synthesizing ability in the GGR-TM_{LIL3} or GGR-TM_{APX} expressing lines.

Substitution of the LHC motif with the TM_{APX} domain in the LIL3 protein stabilizes endogenous GGR - If LIL3 solely functions to anchor GGR to thylakoid membranes, TM_{LIL3} could be replaced with another membrane-spanning domain without compromising the function of LIL3. We tested this hypothesis by replacing TM_{LIL3} with TM_{APX} in the LIL3:2 sequence and overexpressed this chimeric protein in the *lil3:1/lil3:2* double mutant (see Fig. 4). These transgenic lines are termed LIL3(TM_{APX}) lines and we analyzed three independent LIL3(TM_{APX}) lines in this study. These lines also recovered their growth, which was almost undistinguishable from WT (Fig. 5). Consistent with the recovery of plant growth, these plants accumulated a substantial amount of Chl-phy, which accounts for approximately 60-80% of total Chl contents. In contrast, the amount of Chl-GG decreased from 80% of total Chl contents of the *lil3* double mutant to approximately 10% of the total Chl contents in the LIL3(TM_{APX}) lines (Fig. 7). These results demonstrate that LIL3(TM_{APX}) lines substantially recovered phytol biosynthesizing activity. Among the characterized transgenic lines, the levels of LIL3(TM_{APX}) protein varied (Fig. 7B). Specifically, the level was much lower in the line 5 and 16 of the LIL3(TM_{APX}) expressing lines compared to that of WT. It appears that the level of LIL3(TM_{APX}) is not well correlated with that of GGR in line 16. Nevertheless, accumulation of LIL3(TM_{APX}) increased the stability of endogenous GGR in the LIL3(TM_{APX}) overexpressing lines (Fig. 7A), compared to the *lil3* double mutant. These results show that the TM_{LIL3} domain can be replaced by another membrane anchoring domain which lacks an LHC motif, indicating that membrane-anchoring is a primary function of LIL3. On the contrary, if we consider the observation that the GGR levels are still less in the LIL3(TM_{APX}) expressing plants compared to WT (Fig. 7A), this would suggest that the function of LIL3 is not completely fulfilled with TM_{APX}. It is possible that TM_{APX} interferes with the correct folding of LIL3. Alternatively, TM_{LIL3} may have an extra function to enhance the function of LIL3.

Amino acid substitution in the LHC motif of LIL3 protein partly compromised complex formation and GGR accumulation - In order to gain further insight into the function of TM_{LIL3} which includes the LHC motif, we modified the sequence of the LHC motif within the LIL3:2 protein. Three conserved amino acid residues (E171, N174 and D189) of the LHC motif within the LIL3:2 sequence were all substituted with alanine (A) residues (Fig. 8A). Two of these amino acids (E171 and N174) were selected because they correspond to the conserved chlorophyll-binding amino acid residues in the solved structure of LHC (38, 39). D189 was chosen because it is another positively charged residue within the LHC motif of LIL3:2, and we speculated that it might potentially interact with a Chl molecule. We named the amino acid substituted version of the LIL3:2 protein as LIL3(AAA) and three independent LIL3(AAA)-expressing transgenic *Arabidopsis* lines were selected for subsequent functional characterization. Among them, Line 5 accumulates LIL3 protein to a similar level of WT, while Line 11 shows a lower LIL3 level,

and Line 31 shows a higher LIL3 level (Fig. 8C). It is possible that the varied levels of LIL3(AAA) within three independent lines might be due to a variation in transgene expression which is often caused by a positional effect of transgene insertion into the *Arabidopsis* genome. The growth of Line 31 was recovered and it was undistinguishable from WT, while Lines 5 and 11 were still smaller than WT (Fig. 5). However, both of these lines grew better than the *lil3:1/lil3:2* double mutant (Fig. 5). Consistent with the recovery of the growth, Line 31 accumulated Chl-phy levels that were comparable to WT, while the other two LIL3(AAA) expressing lines had less than WT (Fig. 8D). The endogenous GGR levels were correlated with the Chl-phy levels in the LIL3(AAA) lines (Fig. 8B).

Although Line 31 recovered phytol-synthesizing activity with the LIL3 and GGR levels that greatly exceeded the WT levels, Line 5 accumulated LIL3 and GGR proteins at similar levels as observed for WT. It is important to note that Line 5 did not recover phytol-synthesizing activity to a similar level as WT (Fig. 8D). These results indicate that targeted amino acid substitution in the LHC motif partly compromises the function of LIL3. Although these data do not exclude a possibility that the amino acid modification exerted conformational changes on other parts of LIL3, we think this is unlikely because the experiments with LIL3(TM_{APX}) indicated that the conformation of the TM domain and that of the other part of LIL3 were independent from each other. In the case of cyanobacterial FC, removal of the LHC motif from the FC sequence resulted in the dissociation of the FC dimer into monomers (23). The results led us to hypothesize that the modification of the LHC motif in TM_{LIL3} also affects the oligomerization of LIL3-GGR complexes. Therefore, we analyzed the LIL3-GGR complexes in the LIL3(AAA) lines by BN-PAGE, which was followed by SDS-PAGE and immunoblotting. We found that the larger LIL3-GGR complex, which was estimated to be approximately 170 kD with the HMW Native Marker Kit, almost disappeared in the LIL3(AAA) line. On the other hand, smaller complexes which were estimated to be less than 100 kD (Fig. 9), were observed to increase in the LIL3(AAA) line. Although the exact molecular sizes and subunit compositions of these LIL3-GGR complexes are not known at the present time, modification of the conserved amino acids of the LHC motif was shown to result in partial dissociation of the LIL3-GGR complex. We hypothesize that the observed LIL3-GGR oligomers in the LIL3(AAA) lines reflect the in-vivo functional status of these proteins in thylakoid membranes, and it is not due to an aggregation of these proteins during BN-PAGE analysis. It is because our analysis of the Chl-phy levels in the LIL3(AAA) lines shows that these lines substantially recovered their phytol synthesizing activity, indicating that LIL3-GGR is (at least partly) functional (Fig. 8D). However, it is still possible that LIL3 and GGR form an even larger complex and they are partly dissociated to form the observed complexes during the BN-PAGE analysis. In either case, these results indicate that the LHC motif of LIL3 functions to facilitate stable oligomerization of the proteins.

DISCUSSION

Our previous study confirmed that LIL3 is required for the stabilization of GGR in *Arabidopsis* (16). This finding was unexpected because a few characterized GGR enzymes from prokaryotes and plants have been shown to perform their reactions without requiring the presence of additional proteins (25, 40). The exclusive distribution of LIL3 to the green lineage of photosynthetic eukaryotes also raises the question why only Viridiplantae GGR requires LIL3 (6, 7). Considering that GGRs from various organisms are known to accept multiple substrates, such as GGPP, Chl-GG or 2,3-di-O-geranylgeranylglyceryl phosphate (25, 40), it is reasonable to consider that LIL3 is involved in the supply of certain substrates to the GGR reactions in Viridiplantae. In particular, it is interesting to consider that LIL3 holds the tetrapyrrole groups of the substrates of the GGR reaction with its LHC motif to provide them to GGR. However, findings from the present study do not support this model. Transgenic *Arabidopsis* plants expressing LIL3(TM_{APX}) are still able to synthesize phytylated chlorophyll to significant levels (Fig. 7), demonstrating that the tetrapyrrole-binding

ability (if the LHC motif of LIL3 possesses such an ability) is dispensable for GGR reactions. Instead, it is shown that fusion of the TM_{LIL3} or TM_{APX} to GGR stabilizes GGR in the absence of intact LIL3, indicating that membrane-anchoring is essential for the stabilization of GGR. Taken together, we suggest that the primary function of LIL3 is to tether GGR to membranes, and this function is specifically fulfilled by the TM domain which spans the LHC motif.

On the other hand, we hypothesize that LIL3 conveys another function to support the GGR reactions. The Chl-phy levels in the LIL3(TM_{APX}) and LIL3(AAA) lines are still lower than WT, with the exception for the Line 31 of LIL3(AAA) which accumulates a massive amount of LIL3(AAA) protein and synthesizes nearly 100% of Chl-phy (Fig. 8). These results indicate that modification of the TM(LIL3) domain compromises the function of LIL3. One simple explanation for this observation is that the modification of the TM_{LIL3} domain hampers its interaction with GGR and thus destabilizes GGR. However, this explanation does not seem likely, because similar protein levels for GGR are observed in the LIL3(AAA) lines in relative comparison to WT, and furthermore, a substantial amount of GGR and LIL3(AAA) appear to interact with each other to form a smaller complex (Fig. 9). Instead, it is shown that the amino acid substitution in the TM_{LIL3} domain dissociates the large LIL3-GGR complexes into smaller complexes (Fig. 9). These results indicate that the LHC motif of LIL3 facilitates the formation of the native LIL3-GGR complexes, whose size is estimated to be 160 kD or above. In good accordance with these results, it is shown that the TM domains containing the LHC motif have been shown to be essential in oligomerization of other LIL or LHC proteins. The TM domain of cyanobacterial FC, which contains an LHC motif, is functionally involved in the dimerization of FC *in vitro* (22). Two transmembrane helices of LHC, both of which contains an LHC motif, are also known to interact with each other to hold a symmetrical structural backbone of LHC (38). Furthermore, it is suggested that two pairs of cyanobacterial LIL proteins, ScpB/E and ScpC/D, form heterodimers (28). Taking these observations into account, it is possible that one of a fundamental function of LHC motifs is to facilitate the oligomerization of proteins.

Although GGR accumulates to the WT level in Line 5 of LIL3(AAA) overexpressing plants, the Chl-phy levels do not show a similar level of recovery as compared to WT. These results indicate that the formation of the large LIL3-GGR complex is essential for the optimal activity of GGR. It is possible to explain these observations by assuming that the formation of the large LIL3-GGR complex facilitates the substrate shuttling between the active sites of each GGR subunit, which may enable efficient consecutive reduction of GGPP to phytyl-PP or Chl-GG to Chl-phy. A substrate shuttling mechanism has been extensively studied with fatty acid synthase (41). This enzyme catalyzes the consecutive elongation of fatty acid chains by shuttling reaction substrates between the symmetrically positioned identical subunits of the enzyme complex (41). A similar substrate-shuttling mechanism has been postulated for the reaction mechanism of uroporphyrinogen III decarboxylase which catalyzes the consecutive reduction of the four side chains of uroporphyrinogen III to form coproporphyrinogen III (42). In our study, most of the transgenic plants overexpressing the modified versions of LIL3 were found to accumulated intermediate substrates of the reactions (Chl-DHGG and Chl-THGG) (Figs. 7 and 8). It is possible that the modified LIL3-GGR complexes cannot efficiently shuttle the intermediate reaction substrates (such as DHGGPP or THGGPP) between active sites. As a result, these modified complexes would release these intermediates into the environments. A substrate shuttling model of the GGR reaction may serve as a basis for future analysis of the GGR reaction mechanism.

Amino acid substitution in the conserved amino acid residues within the LHC motif of LIL3 results in a partial dissociation of the large LIL3-GGR complex into a smaller complex. These results do not necessarily indicate that these conserved residues bind chlorophyll or other pigments. Moreover, we did not detect any pigment binding to the isolated LIL3-GGR complexes. These results are consistent with the observation with cyanobacterial FC, in

which pigment binding was not detected by fluorescence resonance energy transfer (24). On the contrary, other types of cyanobacterial LIL protein, ScpB, ScpC, ScpD, and ScpE have been shown to bind chlorophyll *in vitro* (28). In addition, one of the plant LIL proteins, (ELIP) has been reported to bind photosynthetic pigments (43). The cyanobacterial LIL proteins mentioned above and ELIP are suggested to associate with the photosynthetic apparatus (10-12) or light-harvesting complexes (13). It is possible that a specific set of LIL proteins including ScpB-E proteins and ELIP gain pigment-binding ability. On the contrary, thylakoid localization and interaction with other proteins are apparently common functions of LIL proteins (10, 12, 13, 21, 44). As a result, it is intriguing to consider that an ancestral protein containing an LHC motif is a membrane-localized protein with a superior ability to interact with other proteins, and that this protein may have gained pigment binding ability to evolve to LHC.

In conclusion, we performed a functional analysis of the LIL3 protein and demonstrated that the TM_{LIL3} domain is not essential in the GGR reaction. Instead, by analyzing GGR-TM_{LIL3} and GGR-TM_{APX}-overexpressing plants, we have shown that the membrane-anchoring function of the TM_{LIL3} domain is important for stabilizing GGR. Furthermore, we hypothesize that LIL3 facilitates the formation of the multimeric LIL3-GGR complex, which appears to more efficiently perform reactions that function to catalyze the reduction of GGPP. Taken together, this study provides novel insight into the function of LIL3 and its TM domain containing a characteristic LHC motif. Collectively, these findings have increased our understanding of the function of the LHC motif which is ubiquitous among oxygenic photosynthetic organisms.

REFERENCES

1. Sonnhammer, E., Eddy, S., Birney, E., Bateman, A., and Durbin, R. (1998) Pfam: Multiple sequence alignments and HMM-profiles of protein domains. *Nucleic Acids Res* **26**, 320–322
2. Finn, R. D., Mistry, J., Tate, J., Coggill, P., Heger, A., Pollington, J. E., Gavin, O. L., Gunasekaran, P., Ceric, G., Forslund, K., Holm, L., Sonnhammer, E. L. L., Eddy, S. R., and Bateman, A. (2009) The Pfam protein families database. *Nucleic Acids Res* **38**, D211–D222
3. Green, B., and Pichersky, E. (1994) Hypothesis for the Evolution of 3-Helix Chl a/b and Chl a/c Light-Harvesting Antenna Proteins from 2-Helix and 4-Helix Ancestors. *Photosyn Res* **39**, 149–162
4. Green, B., and Kühlbrandt, W. (1995) Sequence Conservation of Light-Harvesting and Stress-Response Proteins in Relation to the 3-Dimensional Molecular-Structure of Lhcii. *Photosyn Res* **44**, 139–148
5. Jansson, S. (1999) A guide to the Lhc genes and their relatives in Arabidopsis. *Trends Plant Sci* **4**, 236–240
6. Engelken, J., Brinkmann, H., and Adamska, I. (2010) Taxonomic distribution and origins of the extended LHC (light-harvesting complex) antenna protein superfamily. *BMC Evol Biol* **10**, 233
7. Neilson, J. A. D., and Durnford, D. G. (2010) Evolutionary distribution of light-harvesting complex-like proteins in photosynthetic eukaryotes. *Genome* **53**, 68–78
8. Green, B. R., Pichersky, E., and Kloppstech, K. (1991) Chlorophyll a/b-binding proteins: an extended family. *Trends Biochem Sci* **16**, 181-186
9. Liu, Z., Yan, H., Wang, K., Kuang, T., Zhang, J., Gui, L., An, X., and Chang, W. (2004) Crystal structure of spinach major light-harvesting complex at 2.72 Å resolution. *Nature* **428**, 287–292
10. Kufryk, G., Hernandez-Prieto, M. A., Kieselbach, T., Miranda, H., Vermaas, W., and Funk, C. (2008) Association of small CAB-like proteins (SCPs) of Synechocystis sp. PCC 6803 with Photosystem II. *Photosyn Res* **95**, 135–145
11. Yao, D., Kieselbach, T., Komenda, J., Promnares, K., Prieto, M., Tichy, M., Vermaas, W., and Funk, C. (2007) Localization of the small CAB-like proteins in photosystem II. *J Biol Chem* **282**, 267–276
12. Promnares, K., Komenda, J., Bumba, L., Nebesarova, J., Vacha, F., and Tichy, M. (2006) Cyanobacterial Small Chlorophyll-binding Protein ScpD (HliB) Is Located on the Periphery of Photosystem II in the Vicinity of PsbH and CP47 Subunits. *J. Biol. Chem.* **281**, 32705–32713
13. Heddad, M., Noren, H., Reiser, V., Dunaeva, M., Andersson, B., and Adamska, I. (2006) Differential expression and localization of early light-induced proteins in Arabidopsis. *Plant Physiol* **142**, 75–87
14. Funk, C., Lindström, V., and Vermaas, W. (1999) pp. 103–106, Springer Netherlands, Dordrecht
15. Funk, C., and Vermaas, W. (1999) A Cyanobacterial Gene Family Coding for Single-Helix Proteins Resembling Part of the Light-Harvesting Proteins from Higher Plants. *Biochemistry* **38**, 9397–9404
16. Tanaka, R., Rothbart, M., Oka, S., Takabayashi, A., Takahashi, K., Shibata, M., Myouga, F., Motohashi, R., Shinozaki, K., Grimm, B., and Tanaka, A. (2010) LIL3, a light-harvesting-like protein, plays an essential role in chlorophyll and tocopherol biosynthesis. *Proc Natl Acad Sci U S A* **107**, 16721–16725
17. Vavilin, D., Yao, D., and Vermaas, W. (2007) Small Cab-like Proteins Retard Degradation of Photosystem II-associated Chlorophyll in Synechocystis sp. PCC 6803: KINETIC ANALYSIS OF PIGMENT LABELING WITH 15N AND 13C. *J Biol Chem* **282**, 37660–37668
18. Hernandez-Prieto, M. A., Tibiletti, T., Abasova, L., Kirilovsky, D., Vass, I., and Funk, C. (2011) The small CAB-like proteins of the cyanobacterium Synechocystis sp. PCC 6803: their involvement in chlorophyll biogenesis for Photosystem II. *Biochim Biophys Acta* **1807**, 1143–1151

19. Wang, Q., Jantaro, S., Lu, B., Majeed, W., Bailey, M., and He, Q. (2008) The high light-inducible polypeptides stabilize trimeric photosystem I complex under high light conditions in Synechocystis PCC 6803. *Plant Physiol* **147**, 1239–1250
20. Rizza, A., Boccaccini, A., Lopez-Vidriero, I., Costantino, P., and Vittorioso, P. (2011) Inactivation of the ELIP1 and ELIP2 genes affects Arabidopsis seed germination. *New Phytol* **190**, 896–905
21. Heddad, M., and Adamska, I. (2000) Light stress-regulated two-helix proteins in Arabidopsis thaliana related to the chlorophyll a/b-binding gene family. *Proc Natl Acad Sci U S A* **97**, 3741–3746
22. Sobotka, R., Tichy, M., Wilde, A., and Hunter, C. N. (2011) Functional Assignments for the Carboxyl-Terminal Domains of the Ferrochelatase from Synechocystis PCC 6803: The CAB Domain Plays a Regulatory Role, and Region II Is Essential for Catalysis. *Plant Physiol* **155**, 1735–1747
23. Sobotka, R., McLean, S., Zuberova, M., Hunter, C., and Tichy, M. (2008) The C-terminal extension of ferrochelatase is critical for enzyme activity and for functioning of the tetrapyrrole pathway in Synechocystis strain PCC 6803. *J Bacteriol* **190**, 2086–2095
24. Storm, P., Tibiletti, T., Hall, M., and Funk, C. (2013) Refolding and Enzyme Kinetic Studies on the Ferrochelatase of the Cyanobacterium Synechocystis sp. PCC 6803. *PLoS ONE* **8**, e55569
25. Keller, Y., Bouvier, F., d'Harlingue, A., and Camara, B. (1998) Metabolic compartmentation of plastid prenyllipid biosynthesis--evidence for the involvement of a multifunctional geranylgeranyl reductase. *Eur J Biochem* **251**, 413–417
26. Tanaka, R., Oster, U., Kruse, E., Rüdiger, W., and Grimm, B. (1999) Reduced activity of geranylgeranyl reductase leads to loss of chlorophyll and tocopherol and to partially geranylgeranylated chlorophyll in transgenic tobacco plants expressing antisense RNA for geranylgeranyl reductase. *Plant Physiol* **120**, 695–704
27. Rossini, S., Casazza, A. P., Engelmann, E. C. M., Havaux, M., Jennings, R. C., and Soave, C. (2006) Suppression of both ELIP1 and ELIP2 in Arabidopsis does not affect tolerance to photoinhibition and photooxidative stress. *Plant Physiol* **141**, 1264–1273
28. Storm, P., Hernandez-Prieto, M. A., Eggink, L. L., Hoober, J. K., and Funk, C. (2008) The small CAB-like proteins of Synechocystis sp. PCC 6803 bind chlorophyll. In vitro pigment reconstitution studies on one-helix light-harvesting-like proteins. *Photosyn Res* **98**, 479–488
29. Funk, C., and Vermaas, W. (2012) A Cyanobacterial Gene Family Coding for Single-Helix Proteins Resembling Part of the Light-Harvesting Proteins from Higher Plants. *Biochemistry* **38**, 9397–9404
30. Hellens, R. P., Edwards, E. A., Leyland, N. R., Bean, S., and Mullineaux, P. M. (2000) pGreen: a versatile and flexible binary Ti vector for Agrobacterium-mediated plant transformation. *Plant Mol Biol* **42**, 819–832
31. Earley, K., Haag, J., Pontes, O., Opper, K., Juehne, T., Song, K., and Pikaard, C. (2006) Gateway-compatible vectors for plant functional genomics and proteomics. *Plant J* **45**, 616–629
32. Salvi, D., Rolland, N., Joyard, J., and Ferro, M. (2008) Purification and Proteomic Analysis of Chloroplasts and their Sub-Organellar Compartments in *Methods in Molecular Biology* pp. 19–36, Humana Press, Totowa, NJ
33. Wittig, I., Braun, H.-P., and Schägger, H. (2006) Blue native PAGE. *Nat Protoc* **1**, 418–428
34. Kunugi, M., Takabayashi, A., and Tanaka, A. (2013) Evolutionary changes in chlorophyllide *a* oxygenase (CAO) structure contribute to the acquisition of a new light-harvesting complex in Micromonas. *J Biol Chem* **288**, 19330-19341
35. Edgar, R. C. (2004) MUSCLE: multiple sequence alignment with high accuracy and high throughput. *Nucleic Acids Research* **32**, 1792
36. Salvi, D., Moyet, L., Seigneurin-Berny, D., Ferro, M., Joyard, J., and Rolland, N. (2011) Preparation of envelope membrane fractions from Arabidopsis chloroplasts for proteomic analysis and other studies. *Methods Mol Biol* **775**, 189–206

37. Yoshimura, K., Yabuta, Y., Tamoi, M., Ishikawa, T., and Shigeoka, S. (1999) Alternatively spliced mRNA variants of chloroplast ascorbate peroxidase isoenzymes in spinach leaves. *Biochem J* **338**, 41–48
38. Liu, Z., Yan, H., Wang, K., Kuang, T., Zhang, J., Gui, L., An, X., and Chang, W. (2004) Crystal structure of spinach major light-harvesting complex at 2.72 Å resolution. *Nature* **428**, 287–292
39. Barros, T., Royant, A., Standfuss, J., Dreuw, A., and Kühlbrandt, W. (2009) Crystal structure of plant light-harvesting complex shows the active, energy-transmitting state. *EMBO J* **28**, 298–306
40. Sasaki, D., Fujihashi, M., Iwata, Y., Murakami, M., Yoshimura, T., Hemmi, H., and Miki, K. (2011) Structure and mutation analysis of archaeal geranylgeranyl reductase. *J Mol Biol* **409**, 543–557
41. Jenni, S., Leibundgut, M., Boehringer, D., Frick, C., Mikolasek, B., and Ban, N. (2007) Structure of Fungal Fatty Acid Synthase and Implications for Iterative Substrate Shuttling. *Science* **316**, 254–261
42. Martins, B. M. (2001) Crystal Structure and Substrate Binding Modeling of the Uroporphyrinogen-III Decarboxylase from Nicotiana tabacum. IMPLICATIONS FOR THE CATALYTIC MECHANISM. *J. Biol. Chem.* **276**, 44108–44116
43. Adamska, I., Roobol-Boza, M., Lindahl, M., and Andersson, B. (1999) Isolation of pigment-binding early light-inducible proteins from pea. *Eur J Biochem* **260**, 453–460
44. Adamska, I. (2000) Stable Insertion of the Early Light-induced Proteins into Etioplast Membranes Requires Chlorophyll *a*. *J Biol Chem* **276**, 8582–8587

Acknowledgements- We thank Sachiko Tanaka for her excellent technical assistance.

FOOTNOTES

*This research was supported by the Ministry of Education, Culture, Sports, Science and Technology, Japan, a Grant-in-Aid for Scientific Research, no. 23570042, and by the Leadership Research Grant of the Institute of Low Temperature Science, Hokkaido University to R.T.

[1]To whom correspondence may be addressed: Institute of Low Temperature Science, Hokkaido University, N19W8, Kita-ku, Sapporo, 060-0819, JAPAN, Tel: +81-11-706-5494; E-mail: rtanaka@lowtem.hokudai.ac.jp

[2]Unpublished results from Kaori Takahashi and Ryouichi Tanaka

[3]The abbreviations used are: BN-PAGE, blue-native polyacrylamide gel electrophoresis; FC, ferrochelatase: GGR, geranylgeranyl reductase: Chl-GG, geranylgeranylated chlorophyll, Chl-DHGG, dihydrogeranylgeranylated chlorophyll: Chl-THGG, tetrahydrogeranylgeranylated chlorophyll: Chl-phy, phytylated chlorophyll: WT, wild type.

FIGURE LEGENDS

FIGURE 1. Schematic representation of the metabolic pathways in which GGR is involved. GGR catalyzes six different reactions indicated in this illustration. GPP: geranyl-diphosphate, GGPP: geranylgeranyl-diphosphate, DHGGPP: dihydrogeranylgeranyl-diphosphate, THGGPP: tetrahydrogeranylgeranyl-diphosphate, Phytyl-PP: phytyl-diphosphate, Chl-GG: geranylgeranylated chlorophyll (in this figure, the structure of chlorophyll a is representatively depicted.), Chl-DHGG:

dihydrogeranylgeranylated chlorophyll, Chl-THGG: tetrahydrogeranylgeranylated chlorophyll, Chl-phy: phytylated chlorophyll, GGR: geranylgeranyl reductase, Chl synthase: chlorophyll synthase

FIGURE 2. (A) SDS-PAGE analysis of the purified LIL3-GGR complexes. M: Molecular weight marker. 1. Protein profile of purified WT extracts as a negative control. 2. Protein profile of the purified extracts from the LIL3-FLAG expressing plant. (B) BN-PAGE analysis of the purified LIL3-GGR complexes. Two molecular weight markers (NativeMark from Invitrogen, and WMW Calibration Kit from GE Healthcare) were run for comparison. 1. Protein profile of purified WT extracts as a negative control. 2. Protein profile of the purified extracts from the LIL3-FLAG expressing plant. (C) Two-dimensional BN-PAGE/SDS-PAGE analysis of the purified LIL3-GGR complexes. For BN-PAGE analysis, the HMW Calibration Kit was used for estimation of the molecular weights and gels were stained with a silver staining kit (Thermo Fisher Scientific Inc.).

FIGURE 3. Suborganellar localization of LIL3 and GGR. Chloroplasts were isolated from 4-week-old WT leaves and fractionated into stroma, envelope membranes and thylakoid membranes. Ten ug of protein was loaded per lane for the analyses with anti-LIL3 and anti-GGR antibodies. Two ug of protein was loaded per lane for the analyses with the other antibodies. Anti-Rubisco antibody (stroma marker), anti-Tic110 antibody (envelope marker), anti-Lhcb1 antibody (thylakoid marker), anti-LIL3 antibody, and anti-GGR antibody were incubated with protein blots and subsequently detected with a Western Lightning Plus Enhanced Chemiluminescence Kit (PerkinElmer).

FIGURE 4. Schematic representation of the postulated structure of the modified GGR or LIL3 protein. Depicted stoichiometry of each subunit is hypothetical. The large globular structure colored in purple represents GGR and the small globular structure colored in yellow depicts the N-terminal domain of LIL3. Yellow or green cylindrical structures represent TM_{LIL3} and TM_{APX}, respectively. The LHC motif in TM_{LIL3} is drawn in orange. (A) Postulated structure of the native LIL3-GGR complex. The structure is drawn as a dimer, but it could be a trimer or other types of oligomers. (B) Postulated structure of GGR-TM_{LIL3}. (C) Postulated structure of GGR-TM_{APX}. (D) Structure of the postulated GGR-LIL3(TM_{APX}) complex. (E) Postulated structure of the LIL3(AAA)-GGR complex, which appears to be much smaller than the native LIL3-GGR complexes.

FIGURE 5. Appearance of 4-week-old *Arabidopsis* transgenic plants expressing GGR-TM_{LIL3}, GGR-TM_{APX}, LIL3(TM_{APX}), and LIL3(AAA) together with the WT and *lil3:1/lil3:2* plants. Three independent transgenic lines are presented for each construct.

FIGURE 6. (A) Immunoblotting analysis of GGR-TM_{LIL3} levels in three independent GGR-TM_{LIL3} expressing lines. (B) Immunoblotting analysis of GGR-TM_{APX} levels in three GGR-TM_{APX} expressing lines. (C) The compositions of Chl *a* derivatives in the GGR-TM_{LIL3} and GGR-TM_{APX} lines. Error bars represent standard deviation. n = 4.

FIGURE 7. (A) Immunoblotting analysis of GGR levels in three independent LIL3(TM_{APX})-expressing lines. (B) Immunoblotting analysis of LIL3(TM_{APX}) levels in three independent LIL3(TM_{APX}) expressing lines. (C) The compositions of Chl *a* derivatives in the LIL3(TM_{APX}) lines. Error bars represent standard deviation. n = 4.

FIGURE 8. (A) Amino acid alignment of representative LIL3 and LHC sequences. The numbers above the alignment indicate the amino acid positions in the *Arabidopsis* LIL3:2 sequence. Chlorophyll-binding ligands in the helices 1 and 3 of Lhcb1 are shown with red circles. (B) Immunoblotting analysis of GGR levels in three independent LIL3(AAA)-expressing lines. (C) Immunoblotting analysis of LIL3(AAA) levels in three independent LIL3(AAA) expressing lines. (D) The compositions of Chl *a* derivatives in the LIL3(AAA) lines. Error bars represent standard deviation. n = 4.

FIGURE 9. Complex formation of GGR and LIL3 in the WT and LIL3(AAA) lines resolved by BN-PAGE/SDS-PAGE. Blots were detected with anti-GGR and anti-LIL3 antibodies.

Figure 1

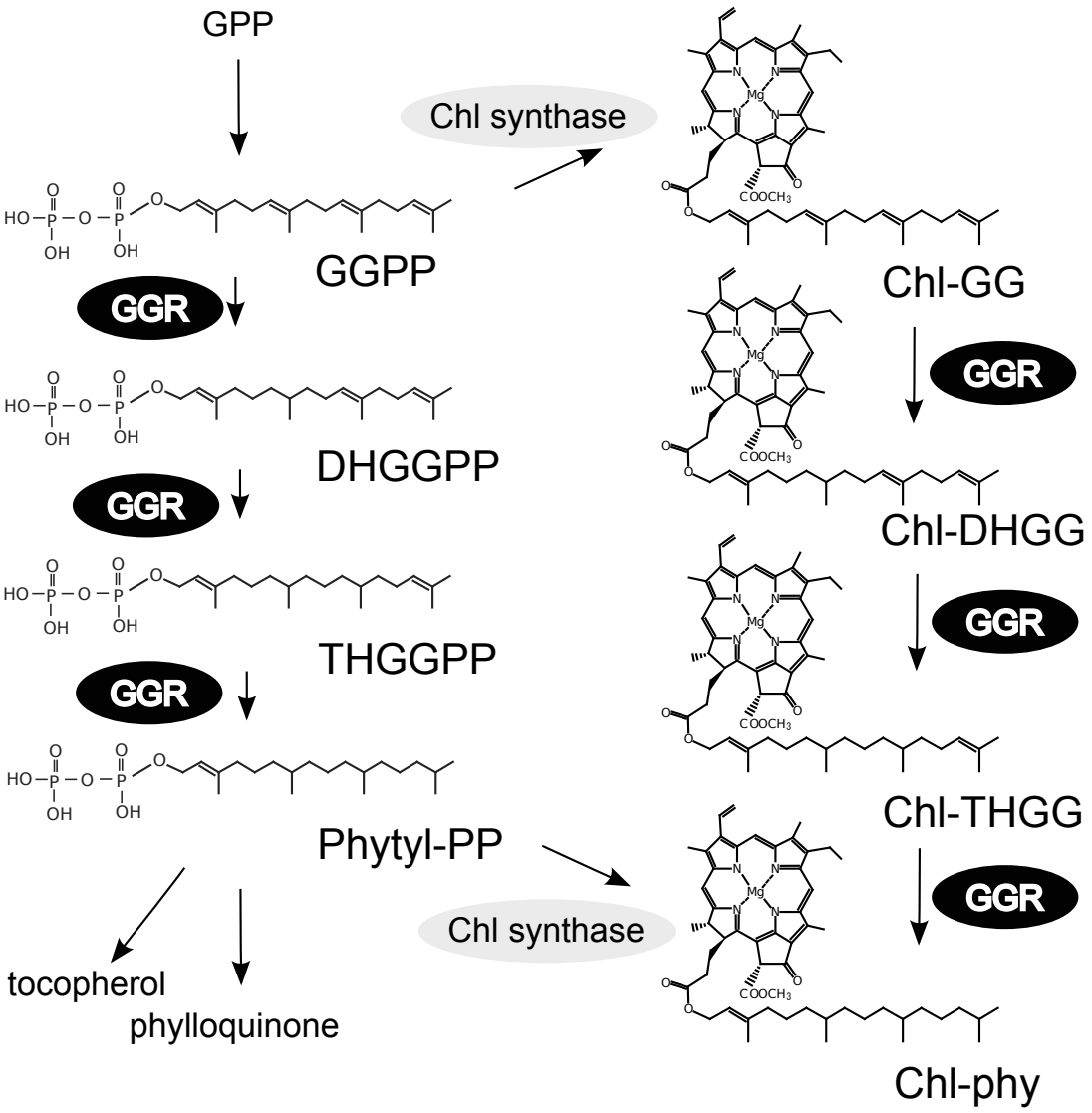
GPP
Chl synthase
GGPP
GGR
DHGGPP
GGR
THGGPP
GGR
Phytyl-PP
tocopherol
phylloquinone
Chl synthase
Chl-GG
GGR
Chl-DHGG
GGR
Chl-THGG
GGR
Chl-phy

Figure 2

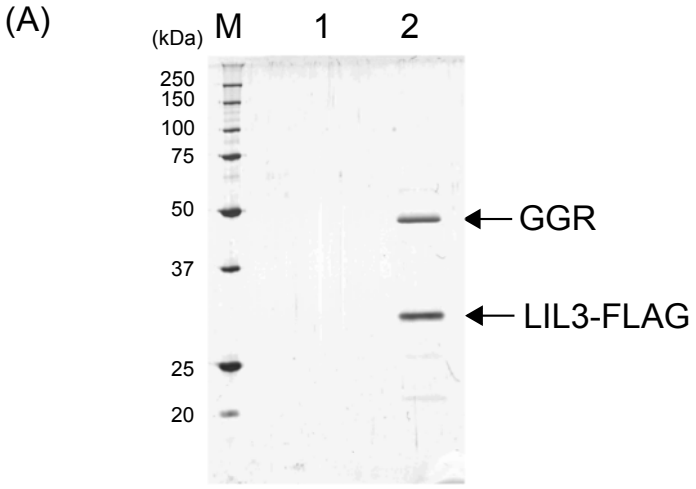
(A)
(kDa)
M
1
2
250
150
100
75
50
37
25
20
GGR
LIL3-FLAG

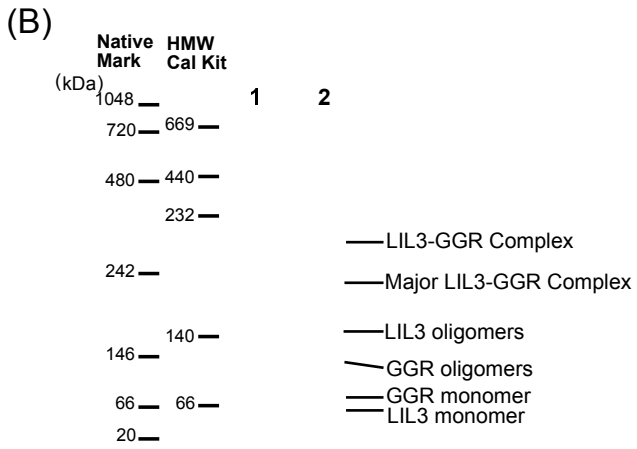
(B)
Native Mark
HMW Cal Kit
(kDa)
1
2
1048
720
669
480
440
232
242
140
146
66
66
20
LIL3-GGR Complex
Major LIL3-GGR Complex
LIL3 oligomers
GGR oligomers
GGR monomer
LIL3 monomer

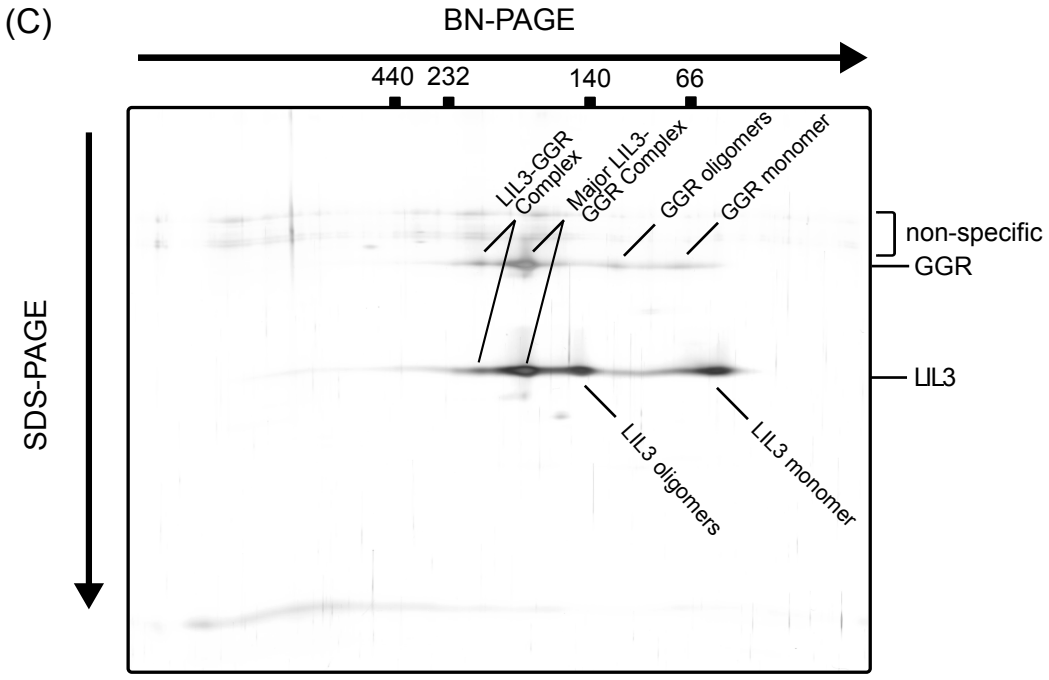
(C)
BN-PAGE
440
232
140
66
SDS-PAGE
LIL3-GGR Complex
Major LIL3-GGR Complex
GGR oligomers
GGR monomer
non-specific
GGR
LIL3
LIL3 oligomers
LIL3 monomer

Figure 3

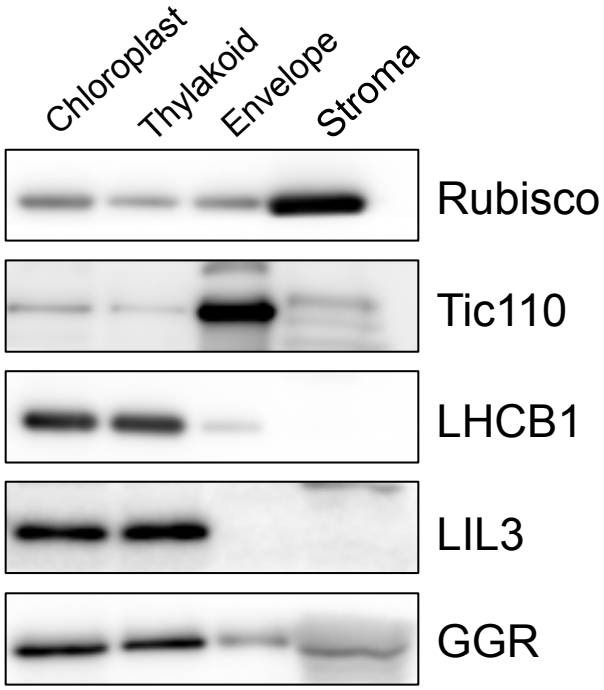
Chloroplast
Thylakoid
Envelope
Stroma
Rubisco
Tic110
LHCB1
LIL3
GGR

Figure 4

(A)

GGR and LIL3 (Wild type)

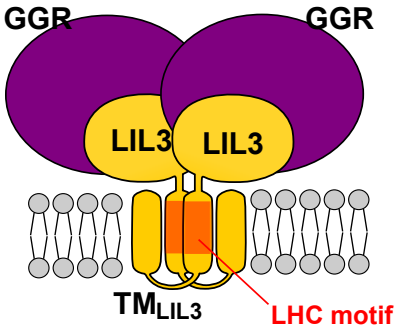

(B)

GGR-TM_{LIL3}

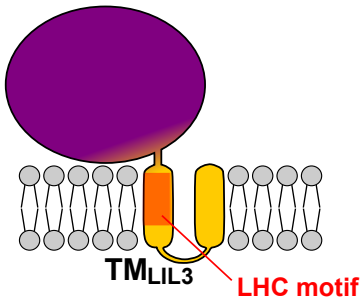

(C)

GGR-TM_{APX}

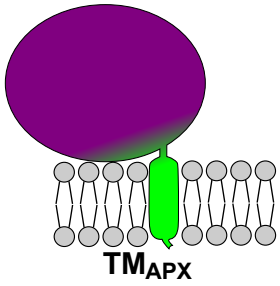

(D)

GGR and LIL3(TM_{APX})

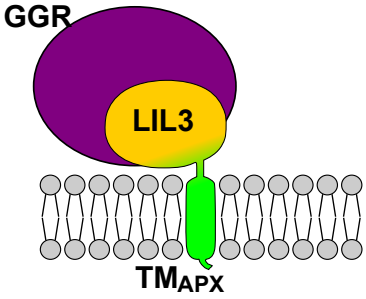

(E)

GGR and LIL3(AAA)

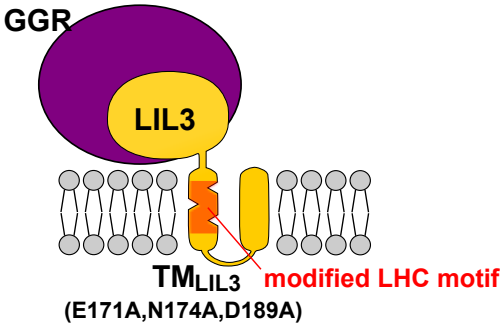

Figure 5

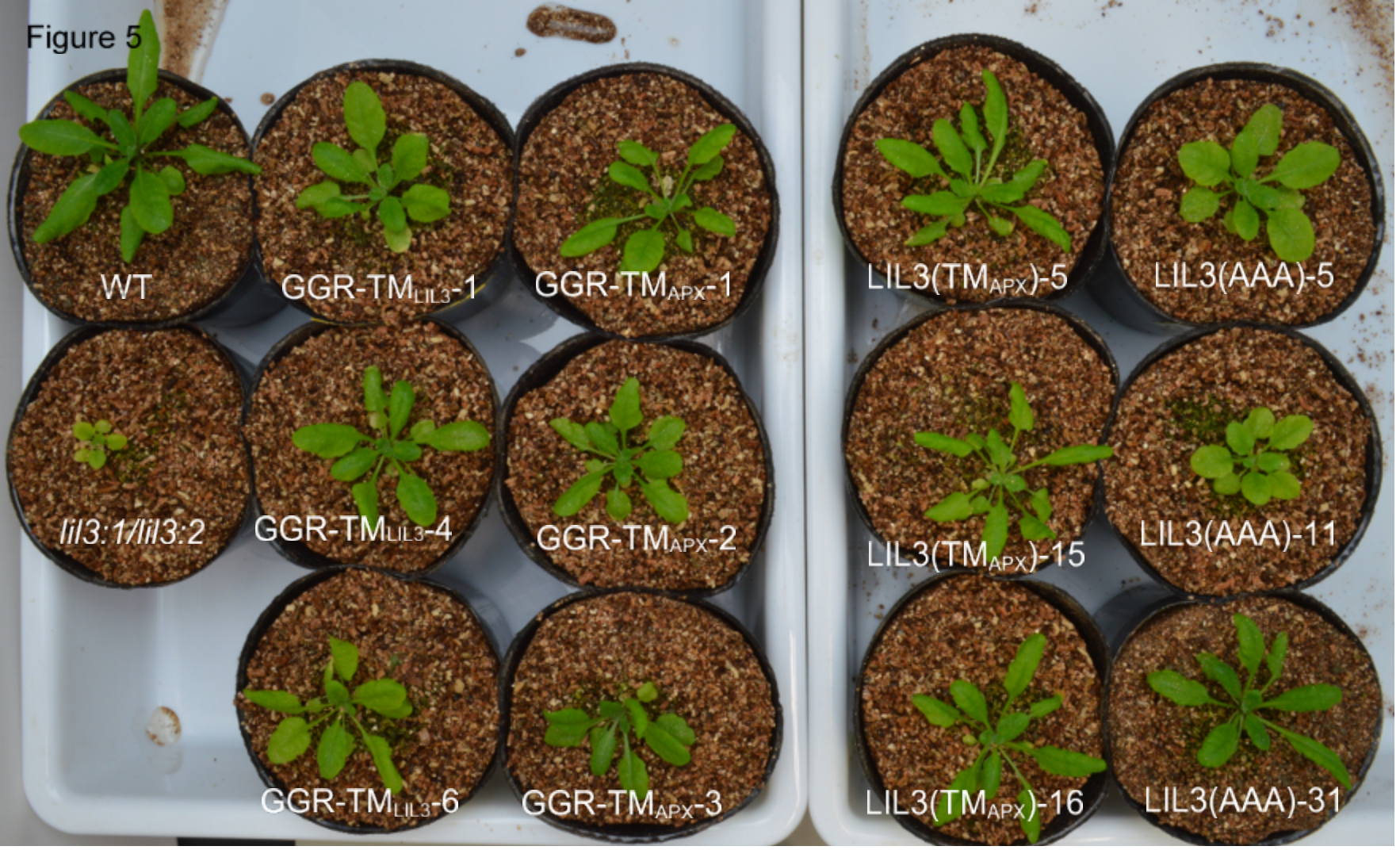
WT
GGR-TM$_{LIL3}$-1
GGR-TM$_{APX}$-1
LIL3(TM$_{APX}$)-5
LIL3(AAA)-5
lil3:1/lil3:2
GGR-TM$_{LIL3}$-4
GGR-TM$_{APX}$-2
LIL3(TM$_{APX}$)-15
LIL3(AAA)-11
GGR-TM$_{LIL3}$-6
GGR-TM$_{APX}$-3
LIL3(TM$_{APX}$)-16
LIL3(AAA)-31

Figure 6

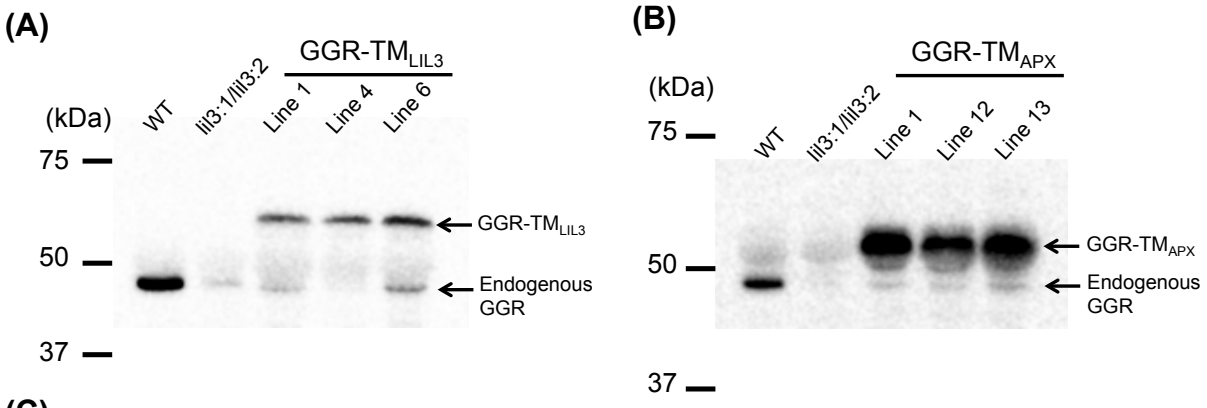
(A)
GGR-TM$_{LIL3}$
(kDa)
WT
lil3:1/lil3:2
Line 1
Line 4
Line 6
75
50
37
GGR-TM$_{LIL3}$
Endogenous GGR
(B)
GGR-TM$_{APX}$
(kDa)
WT
lil3:1/lil3:2
Line 1
Line 12
Line 13
75
50
37
GGR-TM$_{APX}$
Endogenous GGR

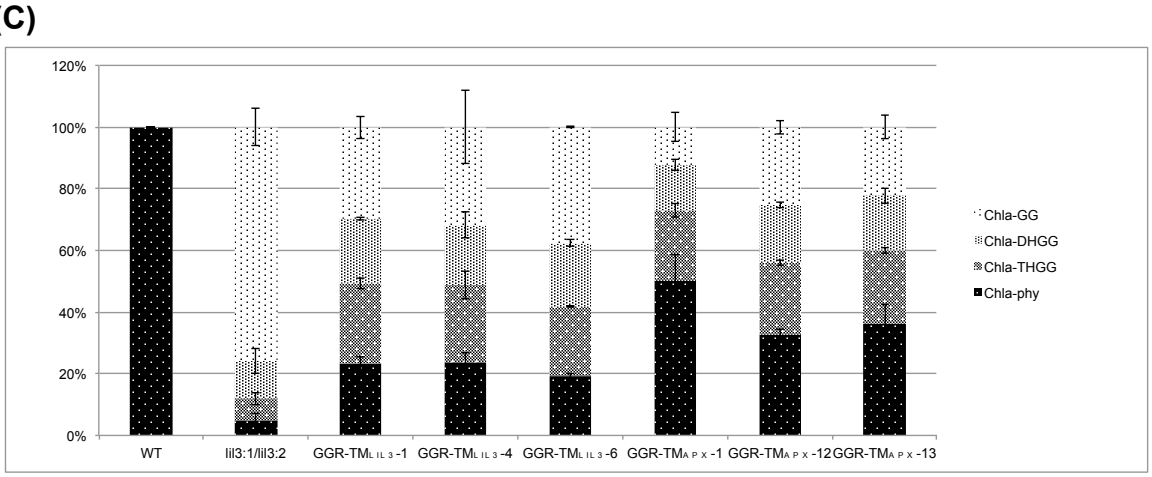
(C)
120%
100%
80%
60%
40%
20%
0%
WT
lil3:1/lil3:2
GGR-TM$_{LIL3}$-1
GGR-TM$_{LIL3}$-4
GGR-TM$_{LIL3}$-6
GGR-TM$_{APX}$-1
GGR-TM$_{APX}$-12
GGR-TM$_{APX}$-13
Chla-GG
Chla-DHGG
Chla-THGG
Chla-phy

Figure 7

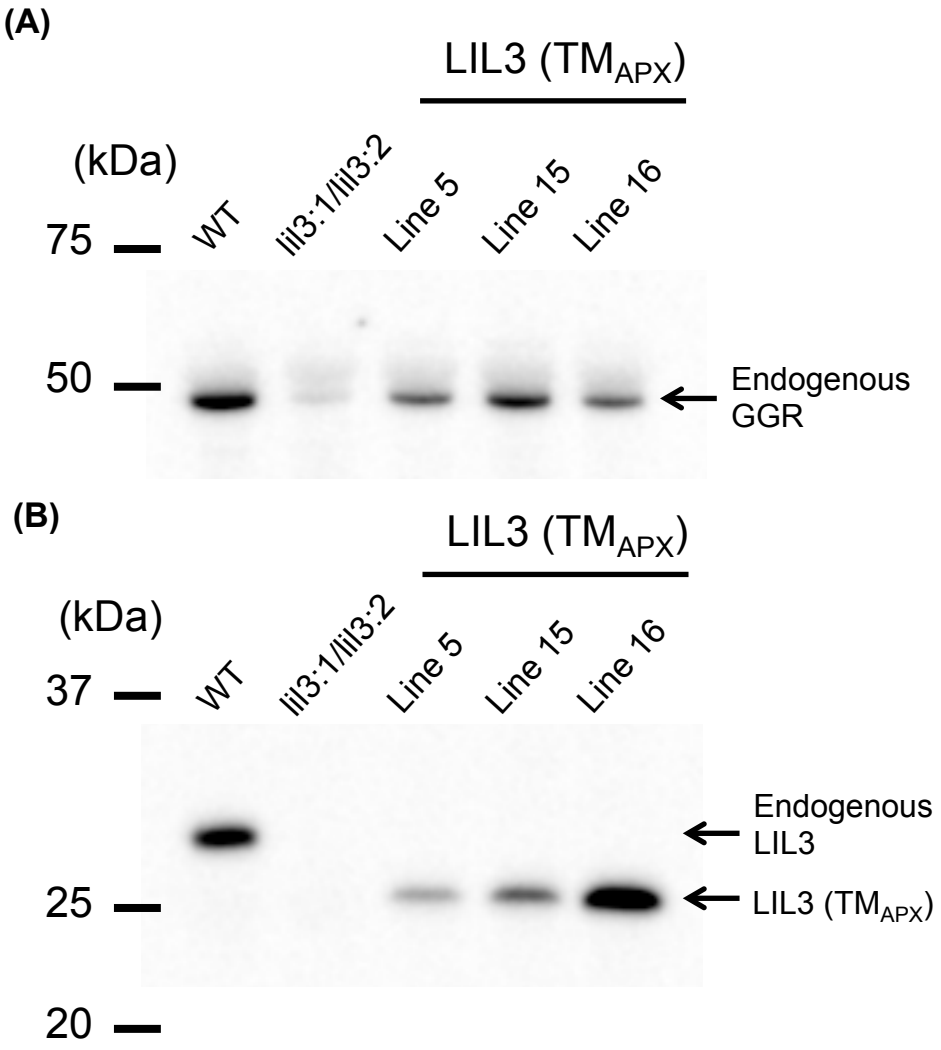
(A)
LIL3 (TMAPX)
(kDa)
WT
lil3:1/lil3:2
Line 5
Line 15
Line 16
75
50
Endogenous GGR
(B)
LIL3 (TMAPX)
(kDa)
WT
lil3:1/lil3:2
Line 5
Line 15
Line 16
37
25
20
Endogenous LIL3
LIL3 (TMAPX)

(C)

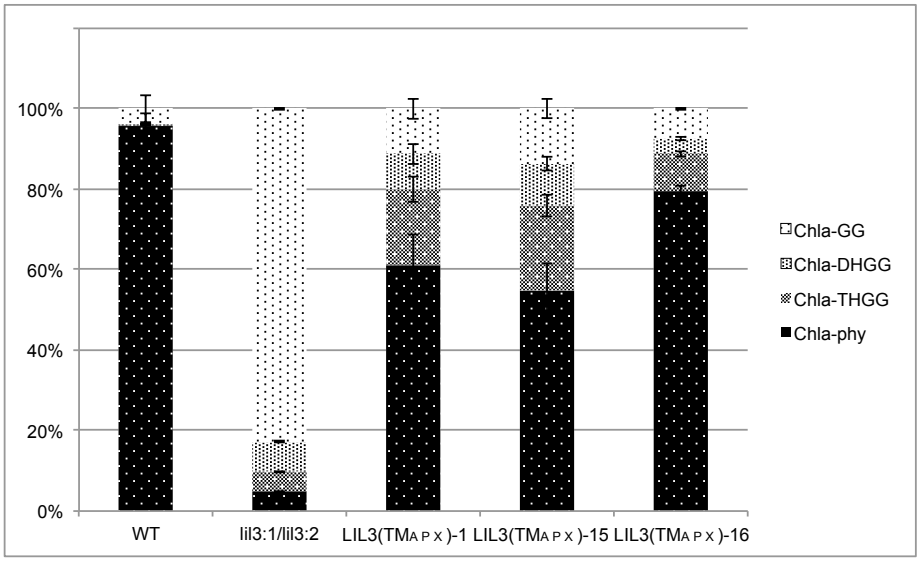
100%
80%
60%
40%
20%
0%
WT
lil3:1/lil3:2
LIL3(TMAPX)-1
LIL3(TMAPX)-15
LIL3(TMAPX)-16
Chla-GG
Chla-DHGG
Chla-THGG
Chla-phy

Figure 8

(A)

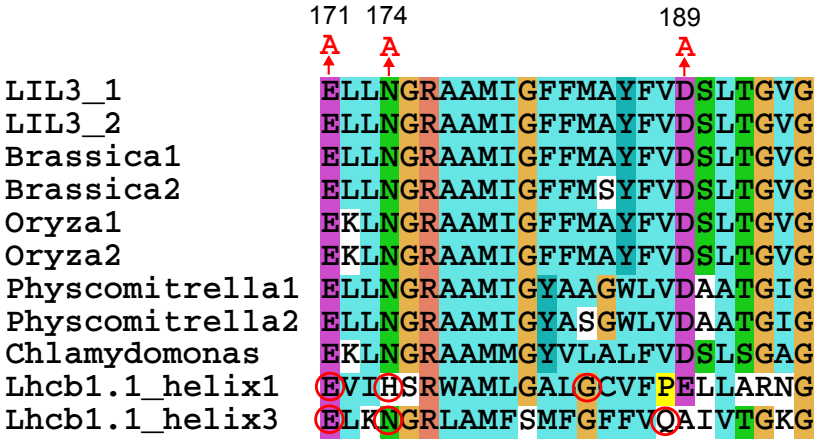

(B)

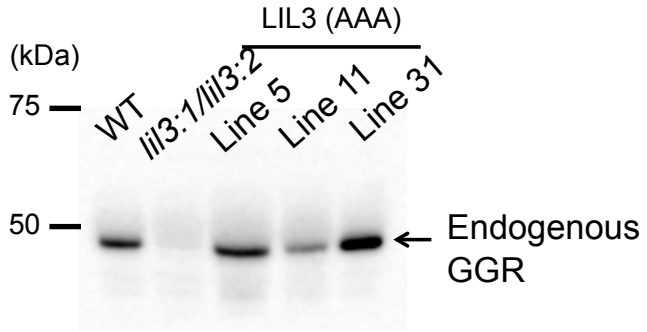

(C)

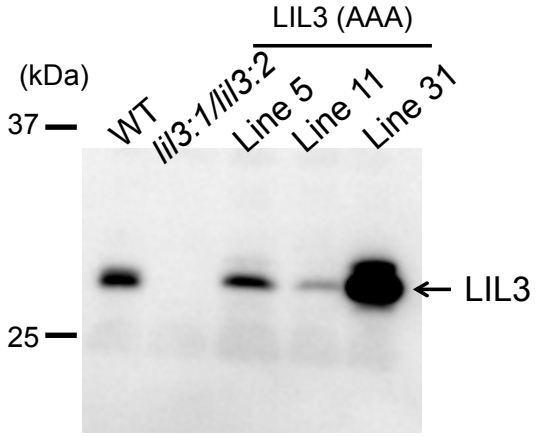

(D)

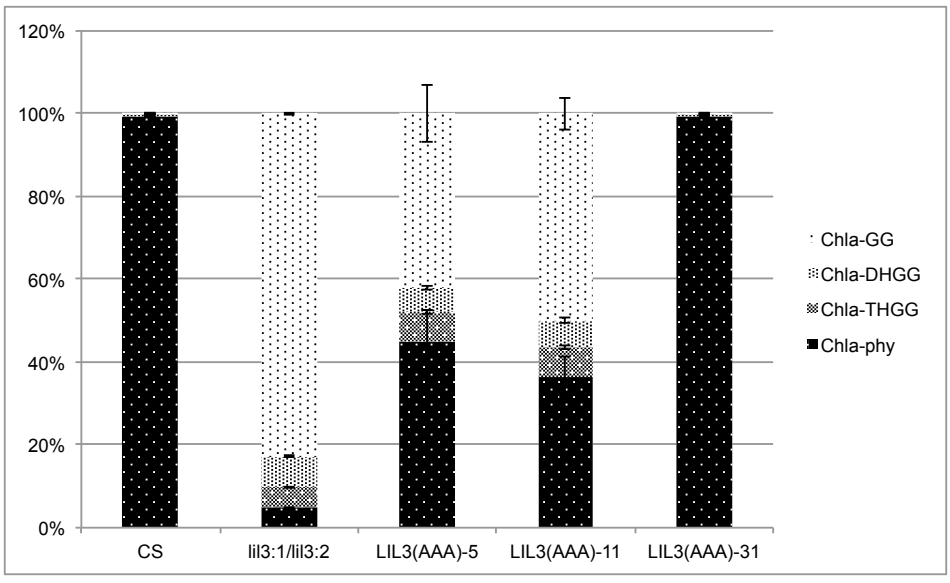

Figure 9

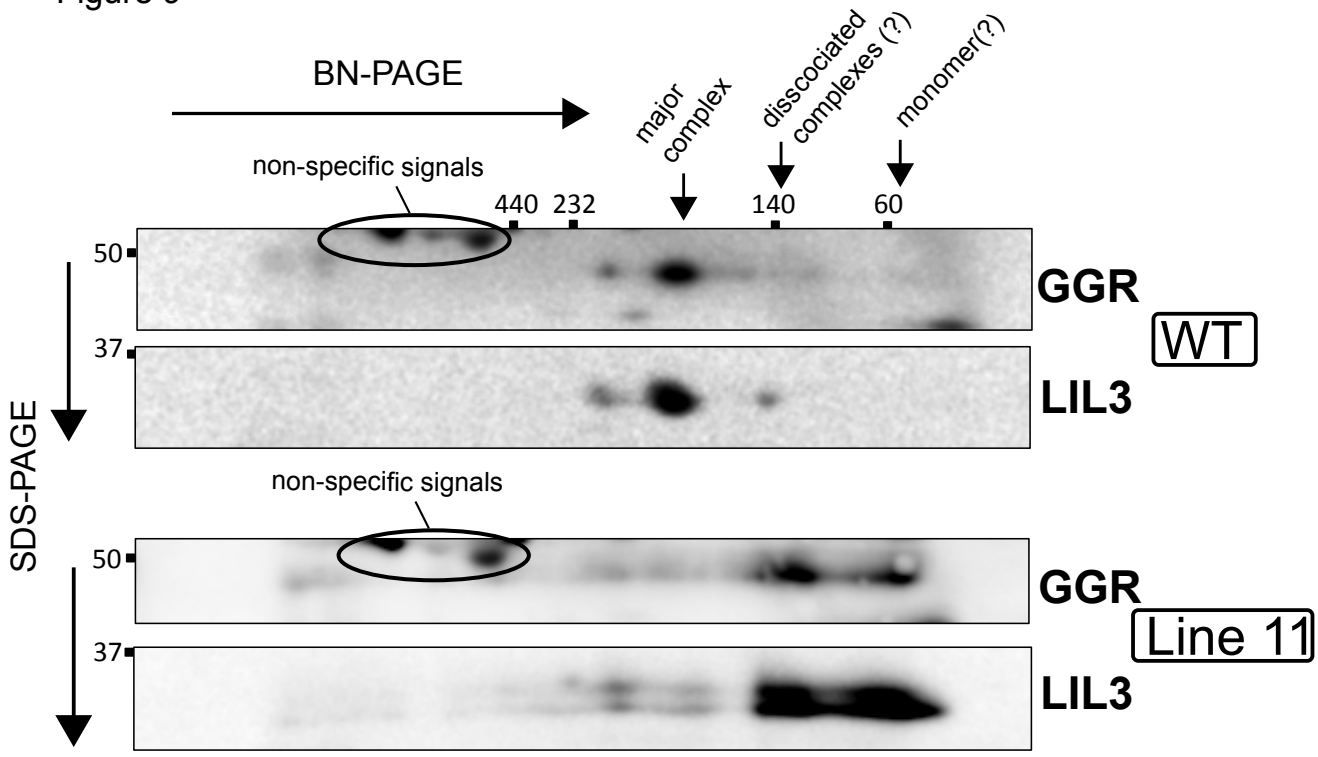
BN-PAGE
major complex
disscociated complexes (?)
monomer(?)
non-specific signals
440
232
140
60
50
37
GGR
WT
LIL3
SDS-PAGE
non-specific signals
50
37
GGR
Line 11
LIL3